



**HAL**  
open science

## Structural features of the adenosine conjugate in means of vibrational spectroscopy and DFT

Kamilla Malek, Edyta Podstawka, Jan Milecki, Grzegorz Schroeder, Leonard M. Proniewicz

► **To cite this version:**

Kamilla Malek, Edyta Podstawka, Jan Milecki, Grzegorz Schroeder, Leonard M. Proniewicz. Structural features of the adenosine conjugate in means of vibrational spectroscopy and DFT. *Biophysical Chemistry*, 2009, 142 (1-3), pp.17. 10.1016/j.bpc.2009.02.007 . hal-00528541

**HAL Id: hal-00528541**

**<https://hal.science/hal-00528541>**

Submitted on 22 Oct 2010

**HAL** is a multi-disciplinary open access archive for the deposit and dissemination of scientific research documents, whether they are published or not. The documents may come from teaching and research institutions in France or abroad, or from public or private research centers.

L'archive ouverte pluridisciplinaire **HAL**, est destinée au dépôt et à la diffusion de documents scientifiques de niveau recherche, publiés ou non, émanant des établissements d'enseignement et de recherche français ou étrangers, des laboratoires publics ou privés.

## Accepted Manuscript

Structural features of the adenosine conjugate in means of vibrational spectroscopy and DFT

Kamilla Malek, Edyta Podstawka, Jan Milecki, Grzegorz Schroeder, Leonard M. Proniewicz

PII: S0301-4622(09)00049-0  
DOI: doi: [10.1016/j.bpc.2009.02.007](https://doi.org/10.1016/j.bpc.2009.02.007)  
Reference: BIOCHE 5235

To appear in: *Biophysical Chemistry*

Received date: 5 November 2008  
Revised date: 19 February 2009  
Accepted date: 19 February 2009

Please cite this article as: Kamilla Malek, Edyta Podstawka, Jan Milecki, Grzegorz Schroeder, Leonard M. Proniewicz, Structural features of the adenosine conjugate in means of vibrational spectroscopy and DFT, *Biophysical Chemistry* (2009), doi: [10.1016/j.bpc.2009.02.007](https://doi.org/10.1016/j.bpc.2009.02.007)

This is a PDF file of an unedited manuscript that has been accepted for publication. As a service to our customers we are providing this early version of the manuscript. The manuscript will undergo copyediting, typesetting, and review of the resulting proof before it is published in its final form. Please note that during the production process errors may be discovered which could affect the content, and all legal disclaimers that apply to the journal pertain.



**Structural features of the adenosine conjugate in means of vibrational spectroscopy and  
DFT**

Kamilla Malek<sup>a</sup>, Edyta Podstawka<sup>a</sup>, Jan Milecki<sup>b</sup>, Grzegorz Schroeder<sup>b</sup> and Leonard M.

Proniewicz<sup>a\*</sup>

<sup>a</sup>Faculty of Chemistry, Jagiellonian Chemistry, 3 Ingardena Str., 30-060 Krakow, Poland

<sup>b</sup>Faculty of Chemistry, Adam Mickiewicz University, 6 Grunwaldzka Str., 60-780 Poznan,  
Poland.

\*Please address all correspondence to Prof. Leonard M. Proniewicz

R. Ingardena 3, 30-060 Krakow, Poland

e-mail: [proniewi@chemia.uj.edu.pl](mailto:proniewi@chemia.uj.edu.pl)

phone: + 48 12 663 22 88

fax: + 48 12 634 05 15

**Abstract**

Vibrational spectra of adenosine bearing benzo-15-crown ether moiety [ $N^6-4'-(benzo-15-crown-5)-adenosine$ , **AC**] have been recorded in solid phase (FT-IR, FT-Raman) and in aqueous solution on the silver colloid surface (SERS). To interpret a very complex vibrational pattern of experimental data, geometrical parameters (molecular structure) as well as harmonic frequencies of the isolated molecule were calculated at the density functional theory level [B3LYP/6-31G(d)]. Assignment of the observed vibrational modes is discussed on the basis of the theoretical results obtained for  $N^6-4'-(benzo-15-crown-5)-adenosine$  as well as its molecular isolated fragments, i.e. adenosine and benzo-15-crown ether. Our analysis of SERS spectrum indicates that adenine and benzo-15-crown ether take tilted orientation while the imino group and ribose adopt almost vertical position in respect to the metal surface. Moreover, calculated atomic charge distribution gives interesting insights into changes of electron density allocation in investigated fragments.

**Keywords:** adenosine, crown ether, IR, Raman, charge distribution, DFT.

## 1. Introduction

Numerous nucleoside conjugates substituted in the different positions serve as tools for studies on structure – functional relationship of nucleic acids. Among them, macrocycles having DNA heterocyclic bases as sidearms play a remarkable role as model molecules in designing molecular reagents, carriers or catalysts [1]. Several important efforts have been reported in this field of DNA modification presenting these conjugates as potential fluorescent reporter groups [2,3], catalytic centers [4,5], surface-binding handles, immune response moieties [6], and prodrugs with anti-HIV activity [7]. In addition, these complexes possess metal ions coordination abilities [8]. Only few of such compounds are available as commercial products. For example, adenosine with crown ether substituted at the N<sup>6</sup> nitrogen atom was reported for the first time from our laboratory [9]. Cation binding affinity of the crown moiety ensures positive charging of the crown residues. Sequence of such modified nucleotides present in an oligonucleotide can by its virtue of the positive charge enhance cell-membrane permeability. This would be additional technique of delivering oligonucleotides (antisense, ribosomes, siRNAs) to the cell. It would constitute another way of improving cellular uptake in addition of known techniques (conjugation with liposomes, cationic polymers, nanoparticles, polylysine peptides, etc.). An attachment of such sequences is possible simply by introducing modified units during oligonucleotide assembly without the need of additional operations necessary when forming hetero-conjugates. Another potential application of the modified adenosine is its use as a carrier of different reporter ions for structural studies [10 and therein].

To be able to plan precisely the use of such complexes for structural studies of oligonucleotides, one has to know as much as possible about steric and electronic properties of modified nucleoside units. These modification can be traced by using different molecular spectroscopy methods as well as X-ray diffraction studies. In this work, we report for the first

time the results of IR (infra red), Raman and SERS (Surface Enhancement Raman Scattering) combined with quantum chemical calculations concerning nucleoside derivative; N<sup>6</sup>-4'-(benzo-15-crown-5)-adenosine (Fig 1.). We show that obtained in this work results are very useful in further structural studies on a new class of compounds: crown ether – nucleoside.

Fragments of elementary building blocks of N<sup>6</sup>-4'-(benzo-15-crown-5)-adenosine (**AC**) such as adenine, ribose and benzo-15-crown ether have been extensively studied in the last decade by using spectroscopic methods. The IR and Raman spectra of adenosine have been previously reported by Navarro and co-workers [11]. They assigned vibrational bands based on classical mechanics and semiempirical methods, whereas Lee et al. [12] measured vibrational spectra of the crystalline adenosine at different temperatures to give an evidence of solid state phase transitions. However, to our best knowledge, there is no publication that deals with normal coordinate analysis of benzo-15-crown ether. Until now, vibrational interpretation of this class of compounds has been carried out by using characteristic frequency groups only [13-15]. Also the possible mechanism of adsorption of all the compounds studied here on different silver and gold surfaces were proposed [13,16-25].

A detail explanation of vibrational structure of such large conjugate is very challenging. However, application of quantum chemical calculations is shown to be an excellent tool to propose description of experimental data. Therefore, in this work extensive calculations of structure, charge distribution and vibrational spectra of the studied molecule are performed at density functional (DFT) level of theory. In addition, to support obtained DFT data for **AC**, its two molecular fragments: adenosine and benzo-15-crown ether were calculated. An analysis of results from molecular structure and charge distribution provides detailed insight into the bonding and electronic changes that take place in N<sup>6</sup>-4'-(benzo-15-crown-5)-adenosine after formation of the conjugate from its individual fragments. Atomic charge is one of the general concepts in chemistry, which gives, in the physical sense, amount

of electronic density gained or lost after formation of a new bond between two atoms. Moreover, atomic charge values can indicate, which molecular atom positions are mainly affected by structural modification of a molecule. This can be used to evaluate, which part of the molecule is mainly involved in delocalisation effect of such electron charge and change of polarity of the bonds. Charge distribution on interfacing surfaces plays also an important role in simulation of electrostatic interactions that contribute to processes involving biomacromolecules. Thus, charge migration along a biomolecule after its chemical change has a particular meaning in prediction its new binding sites due to various noncovalent forces such as salt linkages, hydrogen bonds or hydrophobic interactions.

The next goal of this work is to obtain the clear-cut assignment of the bands observed in the FT-IR and FT-Raman spectra. Thus, theoretical infrared and Raman spectra were calculated to support proposed normal mode assignment. Then, the SER spectrum (on the silver nanocolloidal particles) is explained on the basis of this description. The adsorbate – surface interactions are proposed by identification of frequency shifts of bands emanating from the assigned modes. The SERS method has gained particular importance in recent years in many various research areas, especially in biochemical diagnostic. In general, enhancement of the Raman signal is caused by plasmon excitation through the incident light on the metal surface, and therefore enhanced Raman scattering originating from the fragments of a molecule located on the surface occurs in the spectrum. Since SERS allows for measurements of the very low concentrations ( $\sim 10^{-6}$  M), this method has been used primarily for the detection and recognition of specific fragments of biomolecules, i.e. proteins or nucleic acids. Also the binding behavior of an adsorbate on the metal surface (nanocolloidal particles, films or electrodes) can approximately mimic its interaction with natural receptor site. No other spectroscopic method gives so deep insight in specific molecular interaction with the surface.

## 2. Experimental

**Synthesis.** N<sup>6</sup>-4'-(benzo-15-crown-5)-adenosine was synthesized according to the literature [9].

**FT-IR spectroscopy.** Fourier transform mid-infrared (FT-MIR, 256 scans) spectrum was run in KBr tablet in the spectral range of 400-4000 cm<sup>-1</sup>. It was measured on a Bruker (IFS 48) spectrometer. Resolution was set at 4 cm<sup>-1</sup>.

**FT-Raman spectroscopy.** For FT-Raman measurement, a few milligrams of the compound was placed in glass capillary tube and measured directly; 200 scans were collected (with a resolution of 4 cm<sup>-1</sup>) in the region of 200-4000 cm<sup>-1</sup>. FT-Raman spectrum was recorded on a Bio-Rad step-scan spectrometer (FTS 6000) combined with a Bio-Rad Raman Accessory (FTS 40). Excitation at 1064 nm was made by a Spectra-Physics Topaz T10-106c cw Nd:YAG laser.

**SERS spectroscopy.** AgNO<sub>3</sub> and NaBH<sub>4</sub> were purchased from Sigma-Aldrich Co. (Poznan, Poland) and used without further purification. Three solutions of colloidal silver were prepared according to the standard procedure [26]. Briefly, 8.5 mg of AgNO<sub>3</sub> dissolved in 50 mL deionized water at 4 °C was added drop-wise to 150 mL of 1 mM solution of NaBH<sub>4</sub> immersed in an ice-bath and stirred vigorously. After the addition of AgNO<sub>3</sub> was completed, the resulting pale-yellow solution was stirred and maintained at 4°C for approximately 1 h.

Sample solution (~10<sup>-4</sup> M) was prepared by dissolving **AC** in deionised water. The final sample concentration in the silver colloids was ~10<sup>-5</sup> M.

SERS spectra were measured twice for each batch of the silver colloids with a triple grating spectrometer (Jobin Yvon, T 64000). A liquid-nitrogen-cooled CCD detector (Jobin Yvon, model CCD3000) was used in these measurements. The spectral resolution of 4 cm<sup>-1</sup> was set. The 514.5 nm line (30 mW at the sample) of an Ar-ion laser (Spectra-Physics, model

2025) was used as the excitation source. No spectral changes due to the thermal degradation or desorption process were observed during these measurements.

### Computational Procedures

All calculations were performed using the Gaussian 03 software package [27] at the Academic Computer Center “Cyfronet” in Krakow. As mentioned above, calculations were carried out for N<sup>6</sup>-4'-(benzo-15-crown-5)-adenosine and its basic fragments, i.e. adenosine and benzo-15-crown ether. Investigated in this work molecules are non-planar and belong to the C<sub>1</sub> point symmetry group. Optimized structures, frequencies, and their IR and Raman intensities were calculated using density functional theory (DFT), with Becke three parameter hybrid method and the Lee, Yang, Parr correlation functional (B3LYP) [28,29], with the standard split-valence basis set 6-31G(d). So far, this method has been found to yield geometries, charge distributions, and vibrational spectra of heterocyclic molecules that are in good agreement with experimental data [30-32]. No imaginary frequencies were obtained during optimization. This shows that calculated structures are at their energy minima. Theoretical Raman intensities ( $I^R$ ) were obtained from Gaussian Raman scattering activities (S) according to the expression:  $I_i^R = 10^{-12}(\nu_0 - \nu_i)^4 \nu_i^{-1} S_i$ , where  $\nu_0$  is the excitation frequency (9398.5 cm<sup>-1</sup> for Nd:YAG laser), and  $\nu_i$  is the frequency of the normal mode calculated by DFT [33]. Calculated wavenumbers were multiplied by appropriate scaling factors, i.e. 0.98 and 0.96 for the 0-2000 and 2000-4000 cm<sup>-1</sup> regions, respectively [34,35]. Due to a very complex structure and a large number of normal modes of the title compound, the assignment was made by visual inspection of the modes animated by the Molekel program [36]. To provide the detailed assignment of the calculated IR and Raman spectra, we compared modes of N<sup>6</sup>-4'-(benzo-15-crown-5)-adenosine with these obtained separately for adenosine (potential energy distribution calculated according to [37]) and benzo-15-crown ether (visual

animation). The charge distributions in the compounds were calculated with the Generalized Atomic Polar Tensor scheme [38].

### 3. Results and discussion

#### *Geometry and atomic charge distribution*

The optimized bond lengths and valence angles of N<sup>6</sup>-4'-(benzo-15-crown-5)-adenosine, adenosine, and benzo-15-crown ether are given in Table I (Supplementary Materials). The optimized structures are displayed in Fig. 2. Vibrational spectra of the title compound described further in this work show a good agreement between calculated and experimental results. Hence, the obtained geometry presented here represents preferred structure of **AC**. As mentioned above, the main goal of this part of our study is an investigation of an effect of the individual fragments – adenosine and crown ether – on physico-chemical character of N<sup>6</sup>-4'-(benzo-15-crown-5)-adenosine. According to our calculations, the largest changes in geometry are observed in the crown moiety. The arrangement of the part of the ether ring is changed considerably upon attachment to the adenosine molecule (see Fig. 2 and Table I). Despite many efforts taken to maintain regular structure of this part of the molecule in the optimization process (like in benzo-15-crown ether, c.f. Fig. 2) obtained results were the same leading to the model shown in Fig. 2. It indicates that the binding of the crown moiety to the adenosine molecule twists the former into the irregular shape (c.f. Table I). As a result, the crown C-O bonds in the more distorted fragment lengthen by ~ 0.01 – 0.02 Å (fragment from C<sub>1</sub>'' to C<sub>4</sub>''') while its C-C bonds are affected only slightly (by 0.002 – 0.007 Å). The other C-O bonds elongate by merely ca. 0.002 Å. On the other hand, bond lengths of the “half” phenyl ring (from C<sub>2</sub>'' to C<sub>5</sub>''', clockwise) become shorter by 0.003 – 0.008 Å and the other “half” increases in length by 0.002 – 0.012 Å. Interestingly, the largest alteration concerns bonds (C<sub>4</sub>''-C<sub>5</sub>'' and C<sub>5</sub>''-C<sub>6</sub>'')

adjacent to adenine ( $H_5''-H_6$  distance is 2.26 Å, see Fig. 1). This could be a reason why the further part of benzo-15-crown ether (from  $C_1''$  to  $C_4'''$ , counter-clockwise) is deformed to a greater extent than the fragment from  $C_2''$  to  $O_3'''$  (clockwise). Furthermore, the bond lengths of the adenine ring alter the most by 0.004 Å ( $C_6-N_1$  and  $C_4-N_9$  invariable). Besides, these bonds lengthen and shorten alternately. On the other hand, the sugar residue (ribose) located at the other side of the investigated molecule is the least affected by the presence of crown ether. Here, changes of the bond lengths are negligible (smaller than 0.001 Å).

The atomic charge values are shown in Table II in Supplementary Materials. The GAPT method has been successfully used in proper prediction of charge distribution of many organic compounds and their complexes [39,40]. An analysis of charge distribution fits well with the geometrical changes discussed above. Examination of the results shows that charge changes are smallest for the sugar fragment (less than 0.07 a.u.). Generally, negative as well as positive atomic charges increase simultaneously in this fragment on the individual atoms. The overall charge of the ribose moiety is positive (+0.42 a.u.) and increases insignificantly upon attaching to crown ether by 0.05 a.u.. The excess charge on the  $C_1'-N_9$  bond is congruent with its slight lengthening and concomitant weakening of this bond. Its polarity increases by ~9% in AC. Inspection of the charge distribution in the “pure” adenine molecule (except its amino group) reveals that the total residual charge is close to zero (-0.09 a.u.) and only very small negative charge (0.02 a.u.) is shifted towards the NH group after binding to ether. In addition, the total charge on pyrimidine is highly positive (+0.52 a.u.) while it is quite negative in the imidazole moiety (-0.42 a.u.). Attachment of crown ether causes further accumulation of the positive and negative charges in these rings. However, this indicates rather electron distribution rearrangement (shift from pyrimidine to imidazole) than removing or accepting electron density that appears in the adenine residue. Similarly to the observed charge changes in ribose, the positive and negative charges increase on the individual atoms,

except C<sub>8</sub> (an increase of electron density). This alternation of the charges causes polarity enhancement of the adenine rings' bonds. The greatest differences of the atomic charges are observed for the carbon atoms near the substituted imino group (C<sub>5</sub> and C<sub>6</sub>; by ca. 0.15 a.u.) while the others change by 0.02 – 0.08 a.u., only. Change of the amino group into the imino one provokes significant increase of the negative charge by 23% on the nitrogen atom. In a view of the electron distribution in adenine and benzo-15-crown (discussed below), it seems that the NH group is a barrier-like against a charge flow from adenine to benzo-15-crown and *vice versa*. In benzo-15-crown ether, the carbon and hydrogen atoms of the phenyl group exhibit charges close to zero, except the carbon atoms (C<sub>1</sub><sup>''</sup> and C<sub>2</sub><sup>''</sup>) attached directly to the oxygen atoms (see Fig. 2). This is consistent with typical values found for other organic compounds [38]. Distribution of the charge of the phenyl ring changes drastically after binding of adenosine to the C<sub>4</sub><sup>''</sup> atom and alters charges on the individual atoms depending upon their positions in the ring. The largest charge shift is found for atoms C<sub>3</sub><sup>''</sup>, C<sub>4</sub><sup>''</sup> and C<sub>5</sub><sup>''</sup> since the electron density rises on C<sub>3</sub><sup>''</sup> and C<sub>5</sub><sup>''</sup> over three- and six-times, respectively, and falls on C<sub>4</sub><sup>''</sup> from -0.04 to +0.68 a.u.. The total residual charge of the phenyl ring in benzo-15-crown is positive (+0.79 a.u.). On the other hand, the electron density (0.83 a.u.) is shifted towards atoms that are neighbors of the C<sub>4</sub><sup>''</sup> atom, i.e., the imino group, and the crown ether moiety. In the latter, the electron density increases by ~16%. The most negative charge is accumulated on oxygen (over -4.0 a.u.) and partially on the hydrogen atoms (ca. -1.0 a.u.) while the carbon atoms are strongly positive with the charge of ca. 0.5 a.u.. After complex formation, the electron density is shifted from the hydrogen atoms and the phenyl ring towards the crown oxygen and carbon atoms.

*FT-IR and FT-Raman spectra*

FT-IR and FT-Raman spectra of the complex and its computed counterparts are shown in Figures 3 and 4. Fundamental vibrations of N<sup>6</sup>-4'-(benzo-15-crown-5)-adenosine calculated with the DFT method [B3LYP/6-31G(d)] and their assignment are summarized in Table 1 and compared with the experimental results. Due to the discussed-above molecular structure and the electron density distribution in the title compound, i.e. negligible effect of crown ether on the adenosine moiety, we can safely assume that vibrational modes of both fragments can be analyzed separately. Thus, comparison of the calculated spectra of N<sup>6</sup>-4'-(benzo-15-crown-5)-adenosine and its individual fragments are shown in Figs. I and II (Supplementary Materials). In addition that our assumption is valid, is confirmed by the analysis of their experimental spectra [11-15].

The overall agreement between the experimental and calculated spectra is fairly good. It is supported also by the calculation of the total root mean square error ( $rms_{tot}$ ). Accordingly, the  $rms_{tot}$  is defined as follows:  $rms_{tot} = \left[ \sum_1^n \frac{(\bar{\nu}_i^{theor} - \bar{\nu}_i^{exp})^2}{n} \right]^{1/2}$ , where  $\bar{\nu}_i^{theor}$  and  $\bar{\nu}_i^{exp}$  are the *i*th theoretical scaled and *i*th experimental fundamental frequency (in  $cm^{-1}$ ), respectively; *n* is a number of the mode expected in the spectrum, i.e. 50 and 47 for IR and Raman spectra, respectively. Thus, the  $rms_{tot}$  values are 12 and 13  $cm^{-1}$ , respectively. As is shown, the calculated intensities are in a very good agreement with the experimental data. This agreement is quite pronounced in the Raman spectrum (c.f. Fig. 4).

Because of the complexity of the vibrational modes, the calculated and experimental results for three distinct spectral regions are presented below. Only characteristic modes are discussed in this part. For detail assignment of all the modes observed in IR and Raman see Table 1.

The 3600 to 2800- $cm^{-1}$  Spectral Region

In this region, medium- and weak-intense bands due to OH and CH stretching vibrations are observed in the FT-IR and FT-Raman spectra of the investigated polycrystalline sample (Figs. 3-4). The FT-IR spectrum exhibits a broad band with a maximum at  $\sim 3200\text{ cm}^{-1}$ . The frequency of this band and its FWHM (full width in the half maximum) are due to the presence of existing hydrogen bonding. In addition, some  $\nu(\text{NH})$  stretching modes are expected in this range. Our DFT calculations predicted frequency of  $3434\text{ cm}^{-1}$  for this vibrations but both experimental spectra do not show a distinct band in this region. On the other hand, the absence of this band is confirmed by values of theoretical relative intensities of the mode at  $3434\text{ cm}^{-1}$  which are 0.04 and 0.02 for IR and Raman, respectively. Crystallographic data show [41,42] that intermolecular hydrogen bonding appears in the adenine molecule. Thus, in the case of AC, one has to expect the presence of intra- as well as intermolecular H-bonds that appear in a solid state what complicates enormously our calculations. It has to be mentioned that crystallographic data have not been yet obtained for this type of a molecule. Therefore, the performed calculations correspond only to the isolated molecule of AC. In our calculations, we show that the stretching modes of the free ribose OH group should be observed at the highest frequency range ( $3500\text{-}3300\text{ cm}^{-1}$ ) and it is consistent with the experimental IR spectrum (c.f. Fig.3, Table 1). Then,  $\text{N}^6\text{-}4'\text{-(benzo-15-crown-5)-adenosine}$  can form various H-bonds. Other bands in a spectral region of  $3170\text{-}2880\text{ cm}^{-1}$  result from the stretching vibrations of the CH bonds present in all building blocks of the studied compound (see Table 1). According to our calculations, the isolated modes are attributed to the weak-intensity bands at  $3178\text{ [IR; } \nu(\text{C}_8\text{-H}_8)_{\text{adenine}}]$ ,  $3152\text{ [IR and Raman; } \nu(\text{C}_3\text{'-H}_3\text{'})_{\text{Ph}}]$  and  $2867\text{ cm}^{-1}\text{ [IR; } \nu_s(\text{CH}_2)_{\text{crown}}]$ .

#### The 1700 to $1000\text{ cm}^{-1}$ Spectral Region

Most observed FT-IR and FT-Raman bands in this range are due to the in-plane vibrations of the adenine, phenyl and ribose rings, although they carry significant

contributions from internal coordinates of the crown ether CH<sub>2</sub> groups. Most of these bands are due to the coupled modes of the particular fragments, for example at 1477, 1451, 1378, and 1298 cm<sup>-1</sup> as listed in Table 1. On the other hand, some of the bands we assign to the modes with a more relevant contribution from the individual units of N<sup>6</sup>-4'-(benzo-15-crown-5)-adenosine. Comparison between the vibrational spectra of **AC** and adenosine [11] indicates that the spectra of **AC** are dominated mostly by the adenosine modes. Furthermore, proper frequencies are shifted 5 cm<sup>-1</sup> on average. Only few of them differ in energy by 12-26 cm<sup>-1</sup> and they are discussed below. The observed shifts are, most likely, caused by coupling of the nucleoside vibrations to these of crown ether. Despite close coincidence between proper vibrational modes of the complex and adenosine it has to be emphasized that adenosine “intensity pattern” of several characteristic bands is preserved in the vibrational spectra of the title compound. This is not surprising, since as shown in the charge distribution and geometry part of this work (*vide supra*), after formation of **AC** the atomic charges and bond lengths in adenosine practically do not change considerably. Thus, no significant changes are expected in proper vibrational frequencies. It has to be stressed that such small differences among adequate frequencies and intensities (calculated/experimental) of the modes confirm that suggested theoretical model (calculation performed for the isolated fragments of **AC**) can be straight applied in this study.

Consequently, the IR bands observed at 1655 and 1626 cm<sup>-1</sup> are assigned mainly to the stretches of the carbon-carbon and carbon-nitrogen bonds of adenine. However, small contributions of the out-of-phase C-C stretch of the phenyl group and the in-plane bend of the imino group are also found. In addition, the coupling of the stretching modes of the adenine C-N and the phenyl C-C bonds appear as bands at 1594 (IR and Raman), 1543 (Raman) and 1451 cm<sup>-1</sup> (IR and Raman). These bands have relatively strong intensity in infrared spectrum and very low in Raman (Figs. 3 and 4). As discussed above these IR modes are equivalent to

the pure adenosine absorptions. Relatively smaller contribution to the PED's of the adenine C-N stretches is found for other bands, e.g. 1477 (IR and Raman), 1378 and 1331  $\text{cm}^{-1}$  (IR only). However, Navarro and coworkers [11] and Toyama et al. [43], assign a band at 1331  $\text{cm}^{-1}$  also to a pyrimidine ring vibration. The isolated stretching mode of the single C-N bonds (in-phase vibration) is attributed to a weak-intensity IR band and a very strong Raman band at 1346  $\text{cm}^{-1}$  that is supported by our calculations. The corresponding band in adenosine is observed at 1353  $\text{cm}^{-1}$  (IR and Raman). This proposed assignment is distinct from that suggested Navarro and coworkers [11] who attributed it to the in-plane bending mode of the ribose CCH group. On the other hand, assignment of the pentose modes is troublesome. In the spectral region discussed here, these vibrations are expected to contribute to several bands below 1420  $\text{cm}^{-1}$  and are mainly due to the COH, endo- and exo-cyclic HCO and CCH coupled bending modes. According to our calculations, the bands due to the isolated ribose modes can be located in the spectra at, i.e. IR bands at 1242 (s), 1196 (vw), 1132 (s), 1102 (s), 1082 (m) and 1059 (s)  $\text{cm}^{-1}$  and Raman bands at 1335 (s) and 1132 (w)  $\text{cm}^{-1}$ . Their frequencies overlap with those observed in the adenosine vibrational spectra. Comparison between adenosine and its complex spectra show that new bands are observed in both IR and Raman spectra of N<sup>6</sup>-4'-(benzo-15-crown-5)-adenosine. Thus, it is expected that they associated with the benzo-15-crown ether vibrations. As mentioned above, the stretching modes of the phenyl C-C bonds are coupled with the adenine vibrations and are observed mainly in IR. However, the experimental Raman spectrum exhibits a new very intense band at 1616  $\text{cm}^{-1}$  that we assign to stretches of the CC bonds of the phenyl ring. This mode is found in the unsubstituted crown ether at 1592  $\text{cm}^{-1}$  [13].

The other crown ether modes are observed in the IR spectrum in the 1300 – 1100  $\text{cm}^{-1}$  range. Two relatively strong absorptions at 1264 and 1217  $\text{cm}^{-1}$  are assigned to the twisting mode of CH<sub>2</sub> and stretches of C-O bonds that are formed between the phenyl carbon and

crown oxygen atoms, respectively. Accordingly, two Raman bands that are observed in this region are due to the crown ether vibrations, i.e. the in-phase rocking mode of the phenyl CH group ( $1267\text{ cm}^{-1}$ , vw) and the in-phase CO stretch ( $1171\text{ cm}^{-1}$ , m). Interestingly, the “breathing” mode of the phenyl ring is observed as a medium-intensity IR and a very weak Raman band at  $1030\text{ cm}^{-1}$ . Usually, this mode is observed as a very strong band at ca.  $1000\text{ cm}^{-1}$  in Raman spectrum but not for 1,2,4 trisubstituted derivatives of benzene [44]. Similar spectral pattern was found in the Raman spectrum of the unsubstituted benzo-5-crown ether [13]. Here, its presence in the IR spectrum can be explained by the discussed earlier deformation of the benzo-5-crown moiety upon complex formation with adenosine.

#### The Spectral Region Below $1000\text{ cm}^{-1}$

As listed in Table 1, the isolated modes of the individual fragments of the title compound appear in the range of  $1000 - 450\text{ cm}^{-1}$  and their bands exhibit medium to weak intensities, especially in the Raman spectrum (see Figs. 3-4). Several bands observed between  $850$  and  $450\text{ cm}^{-1}$  are principally assigned to the in- and out-of-plane deformations of the pentose and purine rings. The in-plane bending of ribose appear at  $768$  (m, IR; vw, Raman) and  $565\text{ cm}^{-1}$  (vw, IR) while the out-of-plane vibration of this ring is attributed to a very weak IR band at  $451\text{ cm}^{-1}$ . On the other hand, small contribution of the adenine “breathing”, asymmetric in-plane and out-of-plane bending modes are assigned to a medium IR band at  $789\text{ cm}^{-1}$ , weak IR and Raman bands at  $666$ , and medium IR band at  $637\text{ cm}^{-1}$ , respectively. It is worth-noting that the Raman spectrum does not exhibit any strong intensity band at ca.  $720-730\text{ cm}^{-1}$  deriving from the ring breathing of adenine or adenosine as reported previously [11,12,16].

The crown ether moiety also shows several characteristic vibrations in this spectral region. A strong absorption IR band and a very weak Raman one at  $982\text{ cm}^{-1}$  are due to the out-of-phase stretching mode of the crown part, only. This mode appears also as a very weak

IR and Raman bands at 886 and 824  $\text{cm}^{-1}$  and is coupled to the other vibrations of benzo-5-crown ether (see Table 1). The large contribution of the C-O-C scissoring mode is assigned to the IR and Raman bands at 552 and 513  $\text{cm}^{-1}$ , respectively. The phenyl ring vibrations, which are usually observed below 1000  $\text{cm}^{-1}$ , are due to the CH wagging, in-plane and out-of-plane ring bending modes. They are observed at 860 (w, IR), 750 (w, IR and Raman) and 710  $\text{cm}^{-1}$  (w, IR and Raman), respectively. All the bands discussed here and assigned to benzo-5-crown ether vibrations are absent in the adenosine spectra [11]. The other bands observed in this region result from the coupling of many modes as shown by their PEDs.

### *SERS spectrum*

The SER spectrum of  $\text{N}^6$ -4'-(benzo-15-crown-5)-adenosine adsorbed on the silver colloid surface, in the spectral range of 200-3600  $\text{cm}^{-1}$ , is shown in Fig. 5. The frequencies of the observed SERS bands and their proposed assignment are listed in Table 2. The allocation of the SERS bands to the normal vibrations was done referring to DFT calculations mentioned-above. Also, previously reported assignments of SERS bands reported for adenine [16-18], adenosine [19-22], D-ribose [23] and benzo-5-crown ether [13,24,25] are compared with the analysis presented here. Inspection of Fig. 5 reveals several spectral features. As seen in the figure, strongly enhanced bands are observed in the regions of 2800-3600 and 1150-1650  $\text{cm}^{-1}$ . Below 1150  $\text{cm}^{-1}$  there is a number of very weakly enhanced bands. However, it has to be mentioned that this spectral pattern is reproducible for four independent SERS measurements (two different AC samples, two different preparations of the silver colloid). Comparison between SERS and FT-Raman spectra (cf. Fig. 5 and Table 2) shows that almost all the bands are mainly red-shifted due to adsorption process at the surface of silver colloid. These shifts strongly suggest that the structure of AC differ markedly upon adsorption. All observed in SERS bands are attributed to the different fragment of  $\text{N}^6$ -4'-(benzo-15-crown-5)-

adenosine, i.e., adenine, ribose, benzene, and crown ether that directly are involved in the interaction with the silver surface.

According to our calculations (*vide supra*), the assignment of the bands arising from adenine modes are as follows: 3475  $\text{cm}^{-1}$  [ $\nu(\text{NH})$ ], 3229  $\text{cm}^{-1}$  [ $\nu(\text{C}_8\text{H}_8)$ ], 1569 and 1515  $\text{cm}^{-1}$  [ $\nu(\text{C}=\text{N})$ ,  $\delta(\text{NH})$ ], 1396  $\text{cm}^{-1}$  [ $\omega(\text{NH})$ ], 1333  $\text{cm}^{-1}$  [ $\nu(\text{C}-\text{N})$ ]. The first two high frequency bands (3475 and 3229  $\text{cm}^{-1}$ ) are not observed clearly in the FT-Raman spectrum (not shown in Fig.4) and are assigned based on our calculations. We suggest that SERS enhancement of these modes implies perpendicular orientation of the adsorbed imino group with most probable interaction of the  $\text{C}_8\text{-H}_8$  bond of the nucleoside. On the other hand, all the bands listed above, except these observed above 3000  $\text{cm}^{-1}$ , are present in SERS spectra of adenine and adenosine [16-22] and frequency differences between them and AC (FT-Raman vs. SERS) are not greater than ca. 15  $\text{cm}^{-1}$ .

In addition, it has been previously suggested [16-22] that the SERS band at ca. 1330  $\text{cm}^{-1}$  was attributed to the stretching vibration of the  $\text{C}_5\text{-N}_7$  bond. Such behaviour is characteristic for the vertical position of adenine adsorbed on the silver surface. However, due to restriction of the steric orientation in AC, we do not expect that adenine takes such position in this case. Furthermore, our calculations reveal that a band at 1333  $\text{cm}^{-1}$  should be assigned to coupled stretches of all C-N bonds of adenine. Also, all the SER spectra of adenine and adenosine exhibit a strong band near 730  $\text{cm}^{-1}$ , which has been attributed to the “breathing” mode of the adenine ring. This vibration is much stronger enhanced for vertical orientation of adenine than for flat (parallel) position of this ring [16-22]. Since, as shown in Fig. 5B, this band is absent in the spectrum that may imply practically no interaction of the adenine  $\pi$ -system with the metal surface. To conclude such spectral pattern of AC, we propose that the NH group (the  $\text{N}_6\text{-H}_6$  bond) adopts a vertical position with respect to silver particles, whereas adenine adsorbs in a tilted fashion through the  $\text{C}_8\text{-H}_8$  bond and the  $\text{N}_7$  atom (see Fig. 6).

Another important signal about interaction of **AC** with the silver colloid comes from enhancement of the band at  $3354\text{ cm}^{-1}$ , which is assignable according to our DFT calculation, to the stretching mode of  $\text{O}_2\text{H}$  of ribose. The appearance of this mode suggests that ribose is in intimate contact with the metal surface through the OH groups, and rather weak interactions between the pentose ring and the surface that has been previously reported [20-23]. It is the most likely that other bands arising from  $\nu(\text{OH})$  of ribose are hindered by the broad band at around  $3300\text{ cm}^{-1}$ . Proposed by us orientation of ribose is supported additionally by the presence of the set of bands at: 1358, 1323, 1193, 1141, 1081, and  $843\text{ cm}^{-1}$ , which are attributed chiefly to the bending modes of COH and CCH, and the stretching modes of CC and CO bonds according to our calculations (see Table 2). It seems that the structure of the whole molecule studied here forces the complex to adsorb on the silver surface also by pentose.

Interaction of benzo-15-crown ether moiety with the silver colloid is confirmed by enhancement of the high ( $3201, 2958$  and  $2836\text{ cm}^{-1}$ ) and mid-frequency region bands at  $1628, 1453$  and  $1281\text{ cm}^{-1}$ . Undoubtedly, the band at  $1628\text{ cm}^{-1}$  arises from the in-phase stretches of C-C bonds of the phenyl ring. Hence, its vertical or tilted contact with the metal surface should be considered. Furthermore, examination of the phenyl C-H stretching mode region shows the presence of a very strong band at  $3201\text{ cm}^{-1}$ . According to our DFT calculations, this band is attributed primarily to the stretching mode of the  $\text{C}_3\text{H}_3$  bond. The assignment to this particular CH bond is unquestionable because other CH stretches in the phenyl ring are expected below  $3200\text{ cm}^{-1}$ , i.e. in the region of  $3000\text{-}3070\text{ cm}^{-1}$ . Thus, most likely the phenyl ring is adsorbed in a tilted orientation with respect to the metal surface with a contact mediated by the  $\text{C}_3\text{H}_3$  bond. Obviously, above discussion shows that the crown ether fragment should appear closely to the metal surface. This is confirmed by the enhancement in the SER spectrum several bands due to stretching ( $2958$  and  $2836\text{ cm}^{-1}$ ),

scissoring ( $1453\text{ cm}^{-1}$ ) and twisting ( $1281\text{ cm}^{-1}$ ) modes of the methylene groups. Due to the orientation of the phenyl ring at the surface that imposes some steric hinderence, only a part of crown ether has a chance to interact with the silver surface whereas the other is forced to be exposed to the solution. This is in agreement with the results obtained by Feofanov at al. [13,24] who showed that the unsubstituted benzo-15-crown ether adopts similar to discussed above geometry.

In conclusion, the proposed orientation of  $\text{N}^6\text{-4'-(benzo-15-crown-5)-adenosine}$  adsorbed on the silver colloid is shown in Fig. 6.

#### 4. Conclusions

(1) The vibrational spectra of a novel derivative of adenosine are presented for the first time. These data provide structural information about  $\text{N}^6\text{-4'-(benzo-15-crown-5)-adenosine}$  in solid state (FT-IR and FT-Raman) as well as on the surface of the silver colloid. (2) Comparison of FT-IR and FT-Raman spectra between  $\text{N}^6\text{-4'-(benzo-15-crown-5)-adenosine}$  and its subunits, i.e. adenosine and benzo-15-crown ether, indicates insignificant reorientation and structural changes of the adenosine fragment and essential structural changes of crown ether upon formation of the complex. It is likely that the latter results from the flexibility of the crown bonds and direct substitution to the phenyl ring whereas binding impact on the adenosine moiety is negligible due to the imino group. (3) Observed spectral behavior is consistent with presented here analysis of the geometrical parameters and atomic charge distribution obtained by DFT calculations. Electron density distribution also shows that the NH group prevents charge flowing (lone pair of electrons is located on  $\text{N}_6$ ) between adenosine and benzo-15-crown ether. (4) DFT simulation of vibrational spectra reproduces sufficiently FT-IR and FT-Raman spectra, even though the presence of H-bonding in the solid state was neglected in calculations. However, the calculations of such a simple model allowed

us to give a detailed assignment of all the experimental bands. (5) Comparison of SERS spectrum with the well defined FT-Raman spectrum permits to suggest a binding geometry of N<sup>6</sup>-4'-(benzo-15-crown-5)-adenosine on the metal surface. In our analysis of the SERS experiment, the region of the NH, CH and OH stretching modes occurs to be very helpful and sensitive. SERS enhancements of the several characteristic bands observed in this spectral range evidently define molecular orientation of AC on the metal surface. Finally, we conclude that all the fragments of the complex, i.e. adenine, ribose, benzene and crown ether, adsorb or are very close to the metal layer. Thus, the interaction with the surface takes place mainly through the ribose OH bonds, the adenine C<sub>8</sub>H<sub>8</sub> and NH groups, the phenyl C<sub>3</sub>"H<sub>3</sub>" bond, and the ether CH<sub>2</sub> groups.

### Acknowledgements

The authors thank the Academic Computer Center Cyfronet in Krakow (Poland) for granted computer time (Grant no. MNI/SGI2800/UJ/002/2005). This research was supported by the Ministry of Science and Higher Education (grant no. R05 016 01 to G.S., L.M.P., and K.M.).

### References

1. J. M. Lehn, *Supramolecular Chemistry: Receptors, Catalysts, and Carriers*, Science 227 (1985) 849-856.
2. C. Wagner, M. Rist, E. Mayer-Enthart and H-A. Wagenknecht, 1-Ethynylpyrene-modified guanine and cytosine as optical labels for DNA hybridization, *Org. Biomol. Chem.* 3 (2005) 2062-2063.
3. K. Fujimoto and M. Inouye, DNA duplex-based fluorescence probes/sensors using monomer-excimer switching, *Yakugaku Zasshi – J. Pharm. Soc. Jap.* 128 (2008) 1605-1613.

4. P.G. Schultz, J. Yin and R. A. Lerner, The Chemistry of the Antibody Molecule, *Angew. Chem. Int. Ed.* 41 (2002) 4427-4437.
5. Q. Wang, S. Mikkola and H. Lonnberg, Bimetallic complexes of spiro-azacrown ligands as catalysts of phosphoester and phosphoric anhydride cleavage, *Chem. Biodivers.* 1 (2004) 1316-1326.
6. J. Liu and Y. Lu, Fast Colorimetric Sensing of Adenosine and Cocaine Based on a General Sensor Design Involving Aptamers and Nanoparticles, *Angew. Chem. Int. Ed.* 45 (2006) 90-94.
7. G.T. Morin and B.D. Smith, Crown nucleoside monophosphate diesters: A new class of nucleoside prodrugs, *Tetrahedron Lett.* 37 (1996) 3101-3104.
8. A. Siegel and H. Siegel, Probing of Nucleic Acids by Metal Ion Complexes of Small Molecules (Marcel Dekker, New York, 1996, Vol. 33, pp. 1-678).
9. J. Milecki and G. Schroeder, Adenosine-N6-crown Ethers as a New Class of Ionophores, *Polish J. Chem.* 79 (2005) 1781-1785.
10. R. Juliano, M. Rowshon Alam, V. Dixit and H. Kang, Survey and Summary: Mechanisms and strategies for effective delivery of antisense and siRNA oligonucleotides, *Nucleic Acids Res.* 36 (2008), 4158-4171.
11. L.E. Bailey, R. Navarro and A. Hernanz, Normal coordinate analysis and vibrational spectra of adenosine, *Biospect.* 3 (1997) 47-59.
12. S.A. Lee, A. Anderson, W. Smith, R.H. Griffey and V. Mohan, Temperature-dependent Raman and infrared spectra of nucleosides. Part I – adenosine, *J. Raman Spectrosc.* 31 (2000) 891-896.
13. A. Feofanov, A. Ianoul, V. Oleinikov, S. Gromov, O. Fedorova, M. Alfimov and I. Nabiev, Surface-enhanced resonance Raman spectra of photochromic crown ether

- styryl dyes, their model chromophores, and their complexes with  $Mg^{2+}$ , *J. Phys. Chem.* 100 (1996) 2154-2160.
14. J. Yu, Z. Xu and G. Xu, FT-Raman and FT-IR spectral studies on rare earth complexes with octanedioyl bis(benzo-15-crown-5), *Spectrochim. Acta A* 52 (1996) 1499-1505.
15. F.L. Sousa, F.A. Almeida Paz, P.C.R. Soares-Santos, A.M.V. Cavaleiro, H.I.S. Nogueira, J. Klinowski and T.J. Trindade, Synthesis, characterization and crystal structure of a novel europium(III) supramolecular compound:  $\{[Eu(CH_3OH)_6(H_2O)_2][PMo_{12}O_{40}]\} \cdot (C_{14}H_{20}O_5)_2 \cdot (CH_3OH)_2 \cdot (CH_3CN)_2$ , *J. Mol. Struct.* 689 (2004) 61-67.
16. B. Giese and D. McNaughton, Surface-enhanced Raman spectroscopic and density functional theory study of adenine adsorption to silver surfaces, *J. Phys. Chem. B* 106 (2002) 101-112.
17. C. Otto, F.F.M. de Mul, A. Huizinga and J. Greve, Surface enhanced Raman scattering of derivatives of adenine: the importance of the external amino group in adenine for surface binding, *J. Phys. Chem.* 92 (1988) 1239-1244.
18. J.S. Suh and M. Moskovits, Surface-enhanced Raman spectroscopy of amino acids and nucleotide bases adsorbed on silver, *J. Am. Chem. Soc.* 108 (1986) 4711-4718.
19. T.T. Chen, Y.C. Kuo and N.T. Liang, Surface-enhanced Raman scattering of adenosine triphosphate molecules, *Langmuir* 5 (1989) 887-891.
20. Y.-J. Xiao and J.P. Markwell, Potential dependence of the conformations of nicotinamide adenine dinucleotide on gold electrode determined by FT-Near-IR-SERS, *Langmuir* 13 (1997) 7068-7074.
21. Y.-J. Xiao, Y.F. Chen, T. Wang and X.-X. Gao, Effects of glutamate dehydrogenase enzyme on the SERS spectra of nicotinamide adenine dinucleotide on a gold electrode, *Langmuir* 14 (1998) 7420-7426.

22. S.-P. Chen, C.M. Hosten, A. Vivoni, R.L. Birke and J.R. Lombardi, SERS investigation of NAD<sup>+</sup> adsorbed on a silver electrode, *Langmuir* 18 (2002) 9888-9900.
23. M.F. Mrozek and M.J. Weaver, Detection and identification of aqueous saccharides by using Surface-Enhanced Raman Spectroscopy, *Anal. Chem.* 74 (2002) 4069-4075.
24. A. Feofanov, A. Ianoul, S. Gromov, O. Fedorova, M. Alfimov and I. Nabiev, Complexation of photochromic crown ether styryl dyes with Mg<sup>2+</sup> as probed by Surface-Enhanced Raman Scattering spectroscopy *J. Phys. Chem. B* 101 (1997) 4077-4084.
25. X. Gao, J.P. Davies and M.J. Weaver, Test of surface selection rules for surface-enhanced Raman scattering: the orientation of adsorbed benzene and monosubstituted benzenes on gold, *J. Phys. Chem.* 94 (1990) 6858-6864.
26. E. Podstawka, Y. Ozaki and L.M. Proniewicz, Part I: Surface enhanced Raman spectroscopy investigation of amino acids and their homodipeptides adsorbed on colloidal silver, *Appl. Spectrosc.* 58 (2004) 570-580.
27. Frisch, M. J.; Trucks, G. W.; Schlegel, H. B.; Scuseria, G. E.; Robb, M. A.; Cheeseman, J. R.; Montgomery Jr, J. A.; Vreven, T.; Kudin, K. N.; Burant, J. C.; Millam, J. M.; Iyengar, S. S.; Tomasi, J.; Barone, V.; Mennucci, B.; Cossi, M.; Scalmani, G.; Rega, N.; Petersson, G. A.; Nakatsuji, H.; Hada, M.; Ehara, M.; Toyota, K.; Fukuda, R.; Hasegawa, J.; Ishida, M.; Nakajima, T.; Honda, Y.; Kitao, O.; Nakai, H.; Klene, M.; Li, X.; Knox, J. E.; Hratchian, H. P.; Cross, J. B.; Bakken, V.; Adamo, C.; Jaramillo, J.; Gomperts, R.; Stratmann, R. E.; Yazyev, O.; Austin, A. J.; Cammi, R.; Pomelli, C.; Ochterski, J. W.; Ayala, P. Y.; Morokuma, K.; Voth, G. A.; Salvador, P.; Dannenberg, J. J.; Zakrzewski, V. G.; Dapprich, S.; Daniels, A. D.; Strain, M. C.; Farkas, O.; Malick, D. K.; Rabuck, A. D.; Raghavachari, K.; Foresman, J. B.; Ortiz, J. V.; Cui, Q.; Baboul, A. G.; Clifford, S.; Cioslowski, J.; Stefanov, B. B.; Liu, G.;

- Liashenko, A.; Piskorz, P.; Komaromi, I.; Martin, R. L.; Fox, D. J.; Keith, T.; Al-Laham, M. A.; Peng, C. Y.; Nanayakkara, A.; Challacombe, M.; Gill, P. M. W.; Johnson, B.; Chen, W.; Wong, M. W.; Gonzalez, C.; Pople J. A. Gaussian 03, Revision C.02, Gaussian, Inc., Wallingford CT, 2004.
28. C. Lee, W. Yang and R.G. Parr, Development of the Colle-Salvetti correlation-energy formula into a functional of the electron density, *Phys. Rev. B* 37 (1988) 785-789.
29. A.D. Becke, Density-Functional thermochemistry. 3. The role of exact exchange, *J. Chem. Phys.* 98 (1993) 5648-5652.
30. M.W. Wong, Vibrational frequency prediction using density functional theory, *Chem. Phys. Lett.* 256 (1996) 391-399.
31. K. Zborowski, R. Grybos and L.M. Proniewicz, Vibrational and computational study on maltol (3-hydroxy-2-methyl-4h-pyran-4-one) polymorphism, *Vib. Spectr.* 37 (2005) 233-236.
32. K. Malek, M. Skubel, G. Schroeder, O.P. Shvaika and L.M. Proniewicz, Theoretical and experimental studies on selected 1,3-diazolium salts, *Vib. Spectr.* 42 (2006) 317-324.
33. D. Michalska, and R. Wysokinski, The prediction of Raman spectra of platinum(II) anticancer drugs by density functional theory, *Chem. Phys. Lett.* 403 (2005) 211-217.
34. J. Baker, A.A. Jarzecki and P. Pulay, Direct scaling of primitive valence force constants: An alternative approach to scaled quantum mechanical force fields, *J. Phys. Chem. A* 102 (1998) 1412-1424.
35. D. Michalska, W. Zierkiewicz, D.C. Bieńko, W. Wojciechowski and T. Zeegers-Huyskens, "Troublesome vibrations" of aromatic molecules in second-order Möller-Plesset and Density Functional Theory calculations: Infrared spectra of phenol and phenol-OD revisited, *J. Phys. Chem. A* 105 (2001) 8734-8739.

36. P. Flükiger, H.P. Lützi, S. Portmann and J. Weber, Molekel 4.0, Swiss Center for Scientific Computing, Manno, Switzerland, 2000.
37. J.M.L. Martin and C. Van Alsenoy, Gar2ped, University of Antwerp, 1995.
38. J. Cioslowski, A new population analysis based on atomic polar tensors, *J. Amer. Chem. Soc.* 111 (1989) 8333-8336.
39. K. Malek, H. Kozłowski and L.M. Proniewicz, Interaction of Na(I), Ni(II) and Cu(II) with 2-cyano-2-(hydroxyimino)acetic acid. Spectroscopic and theoretical studies, *Polyhedron*, 24 (2005) 1175-1184.
40. K. Malek, A. Puc, G. Schroeder, V.I. Rybachenko and L.M. Proniewicz, FT-IR and FT-Raman spectroscopies and DFT modelling of benzimidazolium salts, *Chem. Phys.* 327 (2006) 439-451.
41. T.F. Lai and R.E. Marsh, The crystal structure of adenosine, *Acta Cryst.* B28 (1972) 1982-1989.
42. W.T. Klooster, J.R. Ruble and B. Craven, Structure and thermal vibrations of adenosine from neutron diffraction data at 123 K, *Acta Cryst.* B47 (1991) 376-383.
43. A. Toyama, N. Hanada, Y. Abe, H. Takeuchi and I. Harada, Assignment of adenine ring in-plane vibrations in adenosine on the basis of  $^{15}\text{N}$  and  $^{13}\text{C}$  isotopic frequency shifts and TUV resonance Raman enhancement, *J. Raman Spectrosc.* 25 (1994) 623-630.
44. G. Varsanyi, Assignments for vibrational spectra of 700 benzene derivatives (Akademiai Kiado, Budapest, 1973).

## Figure captions

Fig. 1. Atomic numbering system of N<sup>6</sup>-4'-(benzo-15-crown-5)-adenosine.

Fig. 2. The optimized structures of benzo-15-crown ether (left up), adenosine (right up) and N<sup>6</sup>-4'-(benzo-15-crown-5)-adenosine (down).

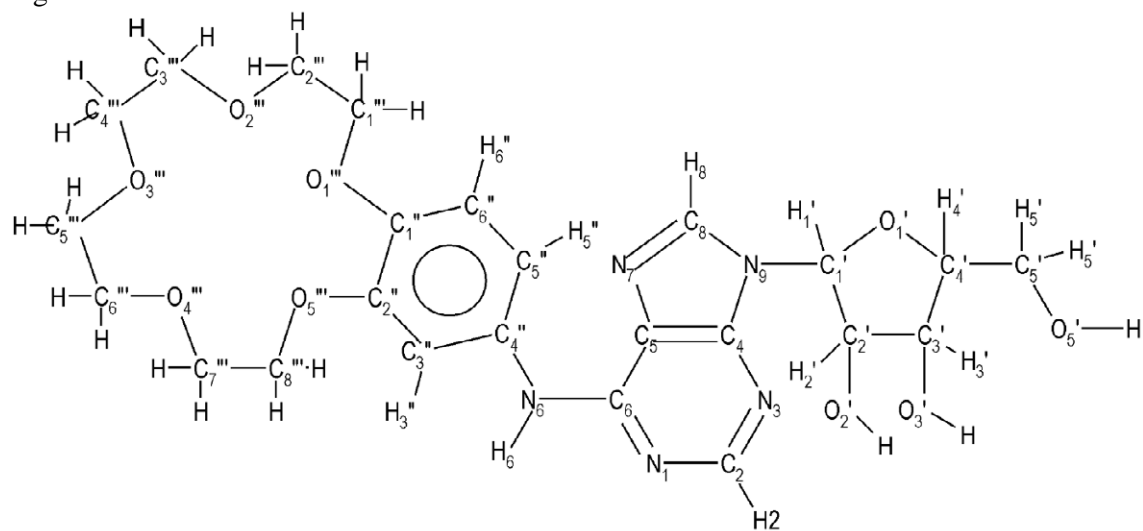
Fig. 3. IR spectra of N<sup>6</sup>-4'-(benzo-15-crown-5)-adenosine A. theoretical, B. experimental.

Fig. 4. Raman spectra of N<sup>6</sup>-4'-(benzo-15-crown-5)-adenosine A. theoretical, B. experimental.

Fig. 5. Comparison of (A) normal Raman spectrum of solid N<sup>6</sup>-4'-(benzo-15-crown-5)-adenosine with (B) SER spectrum for N<sup>6</sup>-4'-(benzo-15-crown-5)-adenosine adsorbed at silver colloidal surface.

Fig. 6. Proposed surface geometry of N<sup>6</sup>-4'-(benzo-15-crown-5)-adenosine adsorbed on the colloid silver.

Fig 1



ACCEPTED M

Fig 2

Figure 2

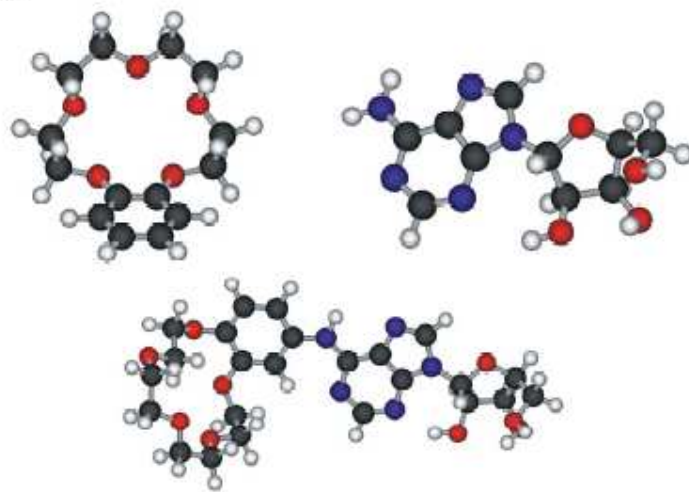


Fig 3

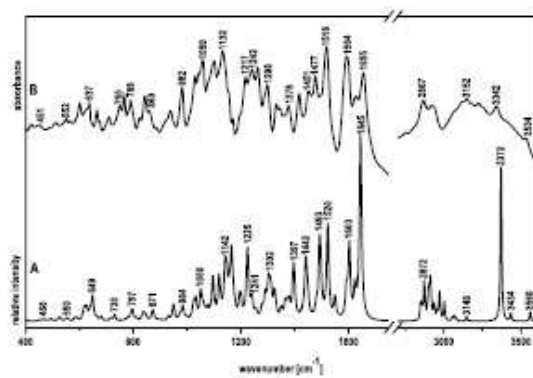


Fig 4

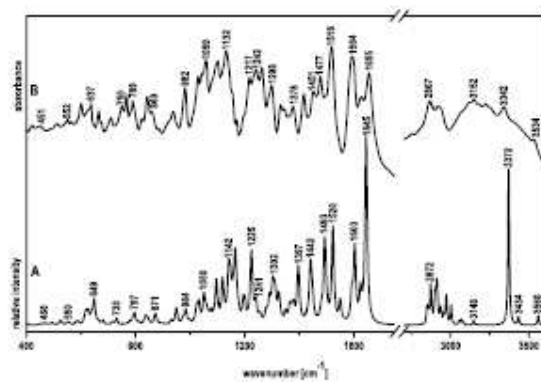


Fig 5

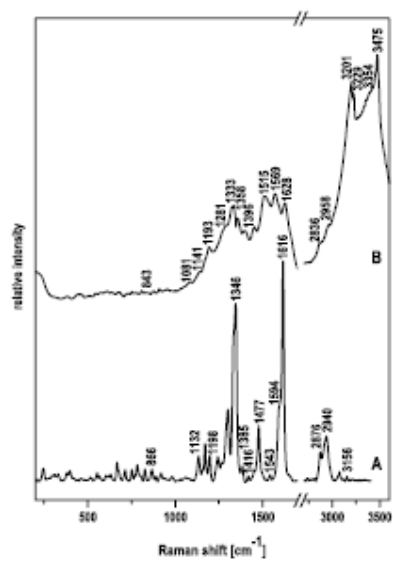


Fig 6

Figure 6



Table 1. The harmonic frequencies (Freq.,  $\text{cm}^{-1}$ ), relative IR and Raman intensities ( $I_{IR}^{rel*}$  and  $I_R^{rel**}$ ) calculated by using B3LYP method [6-31G(d) basis set] and experimental IR and Raman frequencies for N<sup>6</sup>-4'-(benzo-15-crown-5)-adenosine; atom numbering as in Fig. 1.

Experiment		B3LYP/6-31G(d)				Mode
IR	Raman	IR	Raman	$I_{IR}^{rel*}$	$I_R^{rel**}$	
3534vw		3560		0.05	<0.01	$\nu(\text{O}_3\text{H})$
3342w		3371		0.85	<0.01	$\nu(\text{O}_2\text{H})$
3178vw		3170		<0.01	<0.01	$\nu(\text{C}_8\text{H}_8)_{\text{Ad}}$
3152vw	3156vw		3148	0.02	<0.01	$\nu(\text{C}_3''\text{H}_3'')_{\text{Ph}}$
	3075vw		3080/3068		0.02/0.01	$\nu(\text{C}_{5/6}''\text{H})_{\text{Ph,ip}}$ , $\nu(\text{C}_2\text{H}_2)_{\text{Ad}}$
	2940m,br		2934-2977		<0.01-0.03	$\nu_{\text{as}}(\text{CH}_2)_{\text{crown}}$ , $\nu(\text{CH})_{\text{ribose}}$
		2934-3004		0.02-0.08		$\nu_{\text{as}}(\text{CH}_2)_{\text{crown}}$ , $\nu(\text{CH})_{\text{ribose}}$
2921m		2900-2918		0.03-0.08		$\nu_{\text{as}}(\text{CH}_2)_{\text{crown}}$ , $\nu_{\text{s}}(\text{CH}_2)_{\text{crown}}$
	2876m		2848-2912		<0.01-0.04	$\nu_{\text{as}}(\text{CH}_2)_{\text{crown}}$ , $\nu_{\text{s}}(\text{CH}_2)_{\text{crown}}$
2867m		2848-2880		0.02-0.19		$\nu_{\text{s}}(\text{CH}_2)_{\text{crown}}$
1655vs		1645		1.00		$\nu(\text{C}_6\text{-N}_6)_{\text{Ad}}$ , $\nu(\text{C}_4\text{C}_5)_{\text{Ad}}$ , $\nu(\text{CC})_{\text{Ph,op}}$ , $\delta(\text{N}_6\text{H}_6)_{\text{Ad}}$

Experiment		B3LYP/6-31G(d)				Mode
IR	Raman	IR	Raman	$I_{IR}^{rel *}$	$I_R^{rel **}$	
1626m		1603		0.39		$\delta(N_6H_6)_{Ad}$ , $\nu(CC)_{Ph,op}$ , $\nu(CC)_{Ad}$ , $\nu(C_2N_1)_{Ad}$
	1616vs		1624		1.00	$\nu(CC)_{Ph,ip}$
1594vs	1594m,sh		1592	0.14	0.04	$\nu(CC)_{Ph}$ , $\nu(C=N)_{Ad,op}$ , $\delta(N_6H_6)_{Ad}$
	1543w		1550		0.05	$\nu(C=N)_{Ad,ip}$ , $\delta(N_6H_6)_{Ad}$ , $\nu(C_1''C_2'')_{Ph}$ , $\nu(C_3''C_4'')_{Ph}$
1518vs	1520vw		1523	0.43	0.02	$\nu(CC)_{Ph,op}$ , $\delta(CH_2)_{crown,op}$ , $\rho(CH)_{Ph}$
1477m	1477m		1493	0.06	0.02	$\delta(CH_2)_{crown}$ , $\nu(C=N)_{Ad,op}$
1451m	1451vw		1448	0.11	0.22	$\nu(C_2''C_3'')_{Ph}$ , $\nu(C_4C_5)_{Ad}$ , $\nu(C_8N_7)_{Ad}$ , $\nu(C_2N_3)_{Ad}$ , $\nu(C_4''N_6)_{Ad}$
		1441		0.28	0.01	$\rho(C_{2'/3'}H)_{ribose,op}$ , $\delta(C_{2'/3'}OH)_{ribose,op}$
1416m	1416vw		1418	<0.01	0.05	$\omega(C_2H)_{Ad}$ , $\omega(N_6H_6)_{Ad}$
	1385w		1399		0.02	$\rho(CH)_{ribose}$ , $\delta(CH_2)_{crown,op}$ , $\omega(C_2H)_{Ad}$ , $\omega(N_6H_6)_{Ad}$ , $\beta(R_5)_{Ad}$ , $\beta(R_6)_{Ad}$
1378m		1397		0.12		$\delta(CH_2)_{crown,op}$ , $\nu(C_1'N_9)$ , $\nu(C-N)_{Ad,op}$ , $\gamma(CH)_{ribose,op}$
1346w	1346vs		1349	0.04	0.51	$\nu(C-N)_{Ad,ip}$
	1335s,sh		1331		0.07	$\delta(CCH)_{ribose,ip}$ , $\delta(COH)_{ribose,ip}$ , $t(CH_2)_{ribose}$ , $\delta(N_9C_1'H)$ , $\nu(C-N)_{Ad,ip}$
1331m		1325		0.03		$\rho(CH)_{ribose,ip}$ , $\nu(C=N)_{Ad,op}$ , $\rho(C_8H_8)_{Ad}$

Experiment		B3LYP/6-31G(d)				Mode
IR	Raman	IR	Raman	$I_{IR}^{rel *}$	$I_R^{rel **}$	
1298m	1300m		1302	0.09	0.16	$t(CH_2)_{crown,op}$ , $\gamma(C_1'H_1)_{ribose}$ , $\beta_{breathing}(R_5)_{Ad}$ , $\beta_{breathing}(R_6)_{Ad}$ , $\beta_{breathing}(R_6)_{Ph}$
	1267vw		1278		0.08	$\rho(CH)_{Ph,ip}$ , $t(CH_2)_{crown,ip}$
1264s		1257		0.03		$\nu(C_{Ph}-O_{crown})_{op}$ , $t(CH_2)_{crown,op}$
1242s		1241		0.07		$\rho(CH)_{ribose,op}$ , $\rho(C_8H_8)_{Ad}$ , $\delta(COH)_{ribose,op}$
	1244w		1243		0.04	$t(CH_2)_{crown,op}$ , $\rho(CH)_{ribose,ip}$
1217s		1225		0.32		$\nu(C_{Ph}O_{crown})_{op}$ , $\nu(CC)_{Ph,op}$ , $t(CH_2)_{crown,op}$
	1198w		1201		0.05	$\delta(C_5'O_5'H)_{ribose}$ , $\gamma(CH)_{ribose,op}$ , $\rho(CH_2)_{ribose}$ , $\nu(CC)_{benzene,ip}$ , $\nu(C_{Ph}O_{crown})_{op}$
1196vw		1195		0.09		$\gamma(CH)_{ribose,ip}$ , $\rho(CH_2)_{ribose}$ , $\delta(C_5'O_5'H)_{ribose}$
	1171m		1177		0.20	$\nu(CO)_{crown,ip}$ , $\nu(CC)_{benzene,ip}$ , $\beta(R_5)_{Ad}$ , $\beta(R_6)_{Ad}$ , $\gamma(CH)_{ribose,ip}$
1163vw		1165		0.30		$\nu(CO)_{crown,op}$ , $t(CH_2)_{crown,op}$
1156w,sh		1157		0.09		$\nu(CO)_{crown,op}$ , $t(CH_2)_{crown,ip}$
1132s	1132w	1142	1137	0.21	0.04	$\nu(CC)_{ribose}$ , $\nu(CO)_{ribose}$ , $\delta(CCH)_{ribose}$ , $\nu(CO)_{crown}$ , $\rho(CH)_{benzene}$
1102s		1119		0.20		$\nu(C_4'C_5')_{ribose}$ , $\delta(C_5'O_5'H)_{ribose}$
1082m		1096		0.21		$\nu_{as}(C_1'O_1'C_4')_{ribose}$ , $\nu(CO)_{ribose,op}$

Experiment		B3LYP/6-31G(d)				Mode
IR	Raman	IR	Raman	$I_{IR}^{rel *}$	$I_R^{rel **}$	
1059s		1050		0.08		$t(\text{CH}_2)_{\text{ribose}}, \nu_3(\text{C}_1-\text{O}_1-\text{C}_4)_{\text{ribose}}, \nu(\text{CO})_{\text{crown,op}}$
1030m	1030vw		1032	0.10	0.03	$\beta(\text{R}_6)_{\text{Ph}}, \nu(\text{CO})_{\text{crown,ip}}, \nu(\text{CC})_{\text{crown,ip}}$
982s	982vw		984	0.07	<0.01	$\nu(\text{CC})_{\text{crown,ip}}$
938w	938vw		951	0.05	0.02	$\beta_{\text{as}}(\text{R}_5)_{\text{ribose}}, \rho(\text{CH}_2)_{\text{ribose}}$
916w,sh	916vw		906	<0.01	0.02	$\beta(\text{R}_6)_{\text{Ad}}, \beta(\text{R}_5)_{\text{Ad}}$
886vw	886vw		890	<0.01	<0.01	$\nu(\text{C}_7-\text{C}_8)_{\text{crown}}, \beta(\text{R}_6)_{\text{Ph}}$
	866w		874		<0.01	$\nu(\text{C}_2-\text{C}_3)_{\text{ribose}}, \nu(\text{CC})_{\text{crown,ip}}$
860w,sh		871		0.03		$\omega(\text{CH})_{\text{Ph,op}}$
843m		838		0.03		$\nu(\text{CC})_{\text{ribose,ip}}, \nu(\text{CO})_{\text{ribose,op}}, \delta(\text{CCH})_{\text{ribose,op}}$
824w,sh	824vw		833	0.01	0.01	$\nu(\text{CC})_{\text{crown,op}}, \nu(\text{CO})_{\text{crown,ip}}, \rho(\text{CH}_2)_{\text{crown,op}}$
789m		797		0.05		$\beta_{\text{breathing}}(\text{R}_6)_{\text{Ad}}, \beta_{\text{breathing}}(\text{R}_5)_{\text{Ad}}, \beta(\text{R}_5)_{\text{ribose}}, \beta(\text{R}_6)_{\text{Ph}}$
	783w		770		0.18	$\nu(\text{C}_{\text{Ph}}\text{O}_{\text{crown}})_{\text{ip}}, \beta_{\text{as}}(\text{R}_6)_{\text{Ph}}, \rho(\text{CH})_{\text{Ph,op}}$
768m	768vw		762	<0.01	0.02	$\beta_{\text{as}}(\text{R}_5)_{\text{ribose}}$
750w	750w		730	0.03	<0.01	$\beta_{\text{as}}(\text{R}_6)_{\text{Ph}}, \nu(\text{C}_4-\text{N}_6), \nu(\text{C}_{\text{Ph}}\text{O}_{\text{crown}})_{\text{ip}}$

Experiment		B3LYP/6-31G(d)				Mode
IR	Raman	IR	Raman	$I_{IR}^{rel *}$	$I_R^{rel **}$	
710w	710vw		715	0.02	0.01	$\gamma(\mathbf{R}_6)_{Ph}$
666w	666w		681	0.02	0.02	$\beta_{as}(\mathbf{R}_6)_{Ad}, \beta_{as}(\mathbf{R}_5)_{Ad}, \beta_{as}(\mathbf{R}_5)_{ribose}, \beta_{as}(\mathbf{R}_6)_{Ph}$
637m		649		0.13		$\gamma(\mathbf{R}_6)_{Ad}, \gamma(\mathbf{R}_5)_{Ad}, \gamma(\mathbf{O}_2\text{'H})$
	631vw		643		<0.01	$\gamma(\mathbf{R}_6)_{Ad}, \gamma(\mathbf{R}_5)_{Ad}, \beta_{as}(\mathbf{R}_5)_{ribose}, \gamma(\mathbf{N}_6\mathbf{H}_6)_{Ad}, \gamma(\mathbf{C}_8\mathbf{H}_8)_{Ad}$
626w,sh		639		0.04		$\gamma(\mathbf{O}_2\text{'H}), \gamma(\mathbf{N}_6\mathbf{H}_6)_{Ad}, \gamma(\mathbf{R}_5)_{Ad}$
618w,sh	618vw		626	0.06	<0.01	$\gamma(\mathbf{N}_6\mathbf{H}_6)_{Ad}, \gamma(\mathbf{R}_6)_{Ph}$
	605vw		616		<0.01	$\gamma(\mathbf{N}_6\mathbf{H}_6)_{Ad}, \gamma(\mathbf{R}_6)_{Ph}, \gamma(\mathbf{O}_2\text{'H}), \beta_{as}(\mathbf{R}_5)_{ribose}, \beta_{as}(\mathbf{R}_6)_{Ad}, \beta_{as}(\mathbf{R}_5)_{Ad}$
602m		618		0.04		$\gamma(\mathbf{N}_6\mathbf{H}_6)_{Ad}, \gamma(\mathbf{R}_6)_{Ph}, \beta_{as}(\mathbf{R}_5)_{ribose}, \beta_{as}(\mathbf{R}_6)_{Ad}, \beta_{as}(\mathbf{R}_5)_{Ad}$
	567vw		589		0.02	$\delta(\mathbf{C}_1\text{'O}_1\text{'C}_4\text{'})_{ribose}$
565vw		582		0.01		$\beta(\mathbf{R}_5)_{ribose}$
	554vw		555		0.02	$\beta_{as}(\mathbf{R}_6)_{Ad}, \beta_{as}(\mathbf{R}_5)_{ribose}$
552vw		550		<0.01		$\delta(\mathbf{COC})_{crown,op}$
	513vw		532		0.04	$\delta(\mathbf{COC})_{crown,ip}, \beta_{as}(\mathbf{R}_6)_{Ad}$
509vw		526, 524		0.01		$\beta(\mathbf{R})_{crown}, \gamma(\mathbf{C}_{Ph}\mathbf{O}_{crown})_{op}$

Experiment		B3LYP/6-31G(d)				Mode
IR	Raman	IR	Raman	$I_{IR}^{rel *}$	$I_R^{rel **}$	
451vw		466		0.01		$\gamma(\text{OH})_{\text{ribose,op}}, \gamma(\text{R}_5)_{\text{ribose}}$
421vw		450		<0.01		$\gamma(\text{R}_6)_{\text{Ph}}$
	397w		402		0.01	$\gamma_{\text{sym}}(\text{R}_6)_{\text{Ph}}, \nu(\text{CC})_{\text{crown,ip}}$
	380w		388		0.01	$\gamma(\text{C}_5-\text{O}_5)_{\text{ribose}}, \gamma(\text{C}_1-\text{N}_9), \delta(\text{COC})_{\text{crown,ip}}$
	330vw		326		0.02	$\beta(\text{C}_1-\text{N}_9), \beta(\text{C}_6-\text{N}_6)_{\text{Ad}}, \tau(\text{CC})_{\text{crown}}$
	309vw		312		<0.01	$\gamma(\text{R}_6)_{\text{Ad}}, \gamma(\text{R}_5)_{\text{Ad}}, \gamma(\text{R}_6)_{\text{Ph}}, \gamma(\text{C}_{\text{Ph}}\text{O}_{\text{crown}})_{\text{ip}}$
	296vw		286		<0.01	$\delta(\text{C}_{\text{Ph}}\text{O}_{\text{crown}})_{\text{ip}}, \text{butt}_{\text{Ad}}$
	245w		232/227		0.01	$\tau(\text{CC})_{\text{crown}}, \text{butt}_{\text{Ad}}, \tau(\text{C}_4-\text{C}_5)_{\text{ribose}}$

\* relative to the intensity of the band at  $1645 \text{ cm}^{-1}$  ( $794.86 \text{ km}\cdot\text{mol}^{-1}$ ); \*\* relative to the intensity of the band at  $1624 \text{ cm}^{-1}$  (3550.93 arbitrary u.);  $\text{R}_5$  - 5-membered ring;  $\text{R}_6$  - 6-membered ring; Ad - adenine; Ph - the phenyl ring; crown - benzo-15-crown ether; C=N - carbon - nitrogen double bond; C-N - carbon - nitrogen single bond; breathing - breathing mode of the 6-membered ring;  $\nu$  - stretching;  $\delta$  - scissoring;  $\beta$  - bending in-plane;  $\gamma$  - bending out-of-plane;  $\omega$  - wagging;  $\rho$  - rocking;  $t$  - twisting;  $\tau$  - torsion; butt. - butterfly; as - asymmetric; s - symmetric; ip - in-phase; op - out-of-phase; vs - very strong; s - strong; m - medium; w - weak; sh - shoulder.

Table 2. Raman frequencies ( $\text{cm}^{-1}$ ) for  $\text{N}^6$ -4'-(benzo-15-crown-5)-adenosine in solid phase (FT-RS) and adsorbed on silver colloid (SERS).

FT-RS	SERS	Assignment
3434*	3475 vs	$\nu(\text{NH})$
3371*	3354 w	$\nu(\text{O}_2\text{H})$
3178*	3229 s	$\nu(\text{C}_8\text{H}_8)_{\text{Ad}}$
3156 vw	3201 vs	$\nu(\text{C}_3\text{H}_3)_{\text{Ph}}$
2940 m	2958 vw	$\nu_{\text{as}}(\text{CH}_2)_{\text{crown}}, \nu(\text{CH})_{\text{ribose}}$
2876 m	2836 w	$\nu_{\text{as}}(\text{CH}_2)_{\text{crown}}, \nu_{\text{s}}(\text{CH}_2)_{\text{crown}}$
1616 vs	1628 m	$\nu(\text{CC})_{\text{Ph,ip}}$
1594 m,sh	1569 m	$\nu(\text{CC})_{\text{Ph}}, \nu(\text{C=N})_{\text{Ad,op}}, \delta(\text{N}_6\text{H}_6)_{\text{Ad}}$
1543w	1515 m	$\nu(\text{C=N})_{\text{Ad,ip}}, \delta(\text{N}_6\text{H}_6)_{\text{Ad}}$
1477 m	1453 m	$\delta(\text{CH}_2)_{\text{crown}}$
1416 vw	1396 m	$\omega(\text{N}_6\text{H}_6)_{\text{Ad}}$
1385 w	1358 m	$\rho(\text{CH})_{\text{ribose}}, \delta(\text{CH}_2)_{\text{crown,op}}$
1346 vs	1333 m	$\nu(\text{C-N})_{\text{Ad,ip}}$
1335 s,sh	1323 m,sh	$\delta(\text{CCH})_{\text{ribose,ip}}, \delta(\text{COH})_{\text{ribose,ip}}, \text{t}(\text{CH}_2)_{\text{ribose}}$
1267 vw	1281 m	$\rho(\text{CH})_{\text{Ph,ip}}, \text{t}(\text{CH}_2)_{\text{crown,ip}}$
1198 w	1193 m	$\delta(\text{C}_5\text{O}_5\text{H})_{\text{ribose}}, \gamma(\text{CH})_{\text{ribose,op}}$
1132 w	1141 w,sh	$\nu(\text{CC})_{\text{ribose}}, \nu(\text{CO})_{\text{ribose}}, \delta(\text{CCH})_{\text{ribose}}$
1096*	1081 vw	$\nu_{\text{as}}(\text{C}_1\text{O}_1\text{C}_4)_{\text{ribose}}, \nu(\text{CO})_{\text{ribose,op}}$
982 vw	1002 vw	$\nu(\text{CC})_{\text{crown,ip}}$
938 vw	954 vw	$\beta_{\text{as}}(\text{R}_5)_{\text{ribose}}, \rho(\text{CH}_2)_{\text{ribose}}$
916 vw	907 w	$\beta(\text{R}_6)_{\text{Ad}}, \beta(\text{R}_5)_{\text{Ad}}$

886 vw	876 w	$\nu(\text{C}_7^{\text{'''}}\text{C}_8^{\text{'''}})_{\text{crown}}, \beta(\text{R}_6)_{\text{Ph}}$
866 w	843 vw	$\nu(\text{C}_2^{\cdot}\text{C}_3^{\cdot})_{\text{ribose}}, \nu(\text{CC})_{\text{crown,ip}}$
824 vw	807 w	$\nu(\text{CC})_{\text{crown,op}}, \nu(\text{CO})_{\text{crown,ip}}, \rho(\text{CH}_2)_{\text{crown,op}}$
783 w	778 vw	$\nu(\text{C}_{\text{Ph}}\text{O}_{\text{crown}})_{\text{ip}}, \beta_{\text{as}}(\text{R}_6)_{\text{Ph}}, \rho(\text{CH})_{\text{Ph,op}}$
751 w	751 vw	$\beta_{\text{as}}(\text{R}_6)_{\text{Ph}}, \nu(\text{C}_4^{\text{''}}\text{N}_6), \nu(\text{C}_{\text{Ph}}\text{O}_{\text{crown}})_{\text{ip}}$
666 w	679 w	$\beta_{\text{as}}(\text{R}_6)_{\text{Ad}}, \beta_{\text{as}}(\text{R}_5)_{\text{Ad}}, \beta_{\text{as}}(\text{R}_5)_{\text{ribose}}, \beta_{\text{as}}(\text{R}_6)_{\text{Ph}}$
631 vw	636 vw	$\gamma(\text{R}_6)_{\text{Ad}}, \gamma(\text{R}_5)_{\text{Ad}}, \gamma(\text{N}_6\text{H}_6)_{\text{Ad}}, \gamma(\text{C}_8\text{H}_8)_{\text{Ad}}$
618 vw	612 w	$\gamma(\text{N}_6\text{H}_6)_{\text{Ad}}, \gamma(\text{R}_6)_{\text{Ph}}$
567 vw	570 vw	$\delta(\text{C}_1^{\cdot}\text{O}_1^{\cdot}\text{C}_4^{\cdot})_{\text{ribose}}$
554 vw	544 w	$\beta_{\text{as}}(\text{R}_6)_{\text{Ad}}, \beta_{\text{as}}(\text{R}_5)_{\text{ribose}}$
466*	450 br,w	$\gamma(\text{OH})_{\text{ribose,op}}$
380 w	383 w	$\gamma(\text{C}_5^{\cdot}\text{O}_5^{\cdot})_{\text{ribose}}, \gamma(\text{C}_1^{\cdot}\text{-N}_9), \delta(\text{COC})_{\text{crown,ip}}$

---

\*DFT values